

## RESEARCH ARTICLE

*Higher Neural Functions and Behavior* **$\alpha$ -Band activity tracks a two-dimensional spotlight of attention during spatial working memory maintenance**David W. Sutterer,  Sean M. Polyn, and Geoffrey F. Woodman

Department of Psychological Sciences, Vanderbilt University, Nashville, Tennessee

**Abstract**

Covert spatial attention is thought to facilitate the maintenance of locations in working memory, and EEG  $\alpha$ -band activity (8–12 Hz) is proposed to track the focus of covert attention. Recent work has shown that multivariate patterns of  $\alpha$ -band activity track the polar angle of remembered locations relative to fixation. However, a defining feature of covert spatial attention is that it facilitates processing in a specific region of the visual field, and prior work has not determined whether patterns of  $\alpha$ -band activity track the two-dimensional (2-D) coordinates of remembered stimuli within a visual hemifield or are instead maximally sensitive to the polar angle of remembered locations around fixation. Here, we used a lateralized spatial estimation task, in which observers remembered the location of one or two target dots presented to one side of fixation, to test this question. By applying a linear discriminant classifier to the topography of  $\alpha$ -band activity, we found that we were able to decode the location of remembered stimuli. Critically, model comparison revealed that the pattern of classifier choices observed across remembered positions was best explained by a model assuming that  $\alpha$ -band activity tracks the 2-D coordinates of remembered locations rather than a model assuming that  $\alpha$ -band activity tracks the polar angle of remembered locations relative to fixation. These results support the hypothesis that this  $\alpha$ -band activity is involved in the spotlight of attention, and arises from mid- to lower-level visual areas involved in maintaining spatial locations in working memory.

**NEW & NOTEWORTHY** A substantial body of work has shown that patterns of EEG  $\alpha$ -band activity track the angular coordinates of attended and remembered stimuli around fixation, but whether these patterns track the two-dimensional coordinates of stimuli presented within a visual hemifield remains an open question. Here, we demonstrate that  $\alpha$ -band activity tracks the two-dimensional coordinates of remembered stimuli within a hemifield, showing that  $\alpha$ -band activity reflects a spotlight of attention focused on locations maintained in working memory.

*alpha; attention; EEG; visual working memory*

**INTRODUCTION**

An emerging view is that EEG  $\alpha$ -band activity (8–12 Hz) directly reflects the focus of covert spatial attention (1, 2) and that this focus of attention facilitates the online maintenance of locations in working memory (3–5). In support of this view is a growing body of work demonstrating that patterns of  $\alpha$ -band activity on the scalp track the polar angle of attended (6–9) and remembered locations relative to fixation (10–14).

A defining feature of covert spatial attention is the facilitation of processing in a region of space such that processing benefits decrease as distance from the attended region of space increases (15–17). The widespread observation of facilitated processing in a subset of the visual field has led to the

generally accepted theory that spatial attention operates like a spotlight (15, 17). One limitation of work connecting  $\alpha$ -band activity to the focus of covert attention is that it is primarily supported by studies in which stimuli are either presented around fixation or in opposite hemifields along the midline. This means that the spatial precision of this attention mechanism could be extremely fine, as you would expect if it is generated by neurons in areas with small, precise receptive fields like homologs of V2 or V4 (18). Or it could be fairly coarse, such as covering entire quadrants of the visual field or entire hemifields, as is common of neurons in higher level visual areas such as neurons in inferotemporal cortex or the frontal eye fields (19, 20). Thus, an important open question is whether patterns of  $\alpha$ -band activity track the precise two-



dimensional (2-D) coordinates of stimuli presented within the same visual hemifield or a coarse representation of quadrants or even larger regions.

On the one hand, it is well known that cortical regions throughout the visual hierarchy contain retinotopic maps that are sensitive to both polar angle and stimulus eccentricity (21, 22).  $\alpha$ -Band activity has been proposed to be linked to functional magnetic resonance imaging (fMRI) blood-oxygen-level dependent (BOLD) activity in areas of the visual and parietal lobes, including areas with small receptive fields (23, 24), and patterns of fMRI BOLD activity in visual and parietal cortex have been found to track both the polar angle and eccentricity of attended and remembered stimuli (25, 26). In addition, recent work has shown that multivariate patterns of  $\alpha$ -band power reflect other properties of covert spatial attention, such as the temporal dynamics of covert spatial orienting and whether attention is focused on a broad or narrow swath of the visual field (7, 27). Taken together, this past work suggests that  $\alpha$ -band activity may directly reflect the focus of covert attention in mid- to lower-level visual areas with precise visual fields that track the two-dimensional coordinates of attended stimuli. This account predicts that it should be possible to decode the location of stimuli that are presented at the same polar angle from fixation within a hemifield (e.g., both stimuli are presented at 45° relative to fixation) when they are presented at different eccentricities.

On the other hand, while  $\alpha$ -band activity has been proposed to reflect fMRI BOLD activity in the visual and parietal lobe (23, 24), analyses linking multivariate patterns of  $\alpha$ -band activity to retinotopic patterns in the visual system have so far only tested patterns of activity corresponding to the angular location of stimuli around fixation (24). In addition, although previous work has shown that it is possible to use patterns of  $\alpha$ -band activity to correctly estimate which of eight specific angular locations around fixation were attended (7, 11), above-chance estimation of these individual location bins could be driven by relatively coarse activation of brain areas. For example, it would be possible to discriminate between the eight locations used in this previous work even if  $\alpha$ -band power reflects activity from neural populations with large receptive fields that correspond to entire quadrants of the visual field because four of the eight location bins span either vertical or horizontal meridians, and patterns of  $\alpha$ -band activity at meridian locations would reflect activation of two neural populations each responding to a different visual quadrant whereas locations between meridians would reflect activation corresponding to a single quadrant. Moreover, evidence for whether  $\alpha$ -band power tracks the eccentricity of stimuli from fixation has been inconclusive, with some studies showing that  $\alpha$ -band power tracks the eccentricity of items from fixation whereas others have found that it does not (28, 29). Also, recent work finds that the same patterns of  $\alpha$ -band power that track locations of stimuli presented around fixation at one eccentricity can be used to reliably reconstruct locations at the same angle relative to fixation at a different eccentricity (9). Thus, the possibility remains that multivariate patterns of  $\alpha$ -band activity on the scalp are sensitive to relatively coarse populations of neural activity that are limited to tracking the polar angle of stimuli from fixation, but are not sensitive to within hemifield eccentricity from fixation. This account predicts that it should not be possible for a classifier to differentiate between the

locations of stimuli that are presented at different eccentricities if they are presented at the same polar angle from fixation.

In the present work, we tested whether  $\alpha$ -band activity tracks the two-dimensional coordinates of remembered locations or if  $\alpha$ -band activity is limited to tracking the polar angle of remembered locations relative to fixation. To answer this question, we used a lateralized spatial estimation task in which observers were centrally cued to remember the location of one or two target dots presented to one side of the screen. Targets were presented without distractors in *experiment 1*, whereas in *experiment 2* observers also ignored the location of distractor dots presented on the uncued side of the screen. We reasoned that if relatively coarse patterns of  $\alpha$ -band responses enable tracking of remembered locations, we would be unable to track the precise location of each stimulus when two stimuli were presented at confusable locations in a single hemifield. Alternatively, if  $\alpha$ -band activity patterns can finely track remembered locations, we would be able to track remembered locations even when they were presented within a single hemifield. By applying a linear discriminant analysis to the topography of  $\alpha$ -band activity on the scalp, we found that we were able to successfully decode remembered locations. Critically, model comparison revealed that the pattern of classifier choices observed across remembered positions was best explained by a model assuming that  $\alpha$ -band activity tracks the two-dimensional coordinates of remembered locations rather than a model assuming that  $\alpha$ -band activity only tracks the polar angle of remembered stimuli relative to fixation. Together these results are consistent with a framework in which these  $\alpha$ -band signals arise in mid- to lower-level visual areas involved in the deployment of covert attention to spatial locations being maintained in working memory.

## METHODS

### Participants

Fifty-nine adults (27 in *experiment 1* and 32 in *experiment 2*; mean age: 22.2 yr, SD: 4.1; 42 female) participated in the study for monetary compensation (\$15/h). All participants reported normal or corrected-to-normal vision and provided written, informed consent; the study protocol was approved by the Vanderbilt University Internal Review Board.

### Participant exclusions for experiment 1.

The target sample size was determined before data collection and was 20 subjects; based on observations from past work, it was determined that 16 subjects is sufficient to obtain robust spatially specific  $\alpha$ -band activity (9, 11, 30). We opted for a slightly larger sample size in case the spatial selectivity of lateralized stimuli was weaker than centrally presented stimuli. Participants were excluded from the final sample of *experiment 1* if fewer than 400 trials remained in either condition after discarding trials contaminated by recording or ocular artifacts (see *Artifact Rejection*). This artifact number exclusion criterion was set during the first half of data collection based on the number of artifact free trials most subjects could complete during the session. Importantly this criterion was set before the preprocessed data were analyzed. Four observers were excluded because too few trials remained

after artifact rejection, and data collection was terminated early for two participants due to excessive artifacts. The final sample included 21 observers (mean age: 21.7 yr, SD: 2.4; 14 female) with an average of 535 (SD = 71) trials for one-item trials and 559 (SD = 74) trials for two-item trials. The final sample included one extra participant because the experiments were scheduled a week in advance and the data from all participants in the final week passed the artifact exclusion criterion.

### Participant exclusions for experiment 2.

The target sample size was determined before data collection and was 30 participants. An increase in sample size relative to *experiment 1* was adopted in case the inclusion of distractor items resulted in reduced spatial selectivity for targets. We made the decision to terminate data collection early (after 26 participants) because the onset of the Covid-19 pandemic precluded further data collection. Participants were excluded from the final sample if fewer than 200 trials per condition remained after discarding trials contaminated by recording or ocular artifacts (see *Artifact Rejection*). This artifact exclusion criterion was decided on before data collection because it resulted in the same number of trials per condition as in *experiment 1* (e.g., 400 trials per set size and 400 trials per hemifield). Three observers were excluded because too few trials remained after artifact rejection, and data collection was terminated early for three participants due to excessive artifacts. The final sample included 26 observers (mean age: 22.6 yr, SD: 5.34; 19 female) with an average of 297 (SD = 45) one-item left-target trials, 301 (SD = 44) one-item right-target trials, 286 (SD = 46) two-item left-target trials, and 288 (SD = 38) two-item right-target trials.

### Apparatus and Stimuli

Participants were tested in a dimly lit, electrically shielded chamber. Stimuli were generated using MATLAB (MathWorks, Natick, MA) and the Psychophysics Toolbox (31, 32) and were presented on a 24 in. LCD monitor (refresh rate: 120 Hz, resolution: 1,080 × 1,920 pixels) at a viewing distance of 75 cm (head position was stabilized with a chinrest). A gray background (40.8 cd/m<sup>2</sup>) and a white fixation dot (0.2° of visual angle in diameter, 13.2 cd/m<sup>2</sup>) appeared in all displays.

### Experiment 1 task procedure and stimuli.

Participants performed a spatial short-term memory task in which they maintained fixation and remembered the position

of one or two stimuli presented to the left of fixation (Fig. 1A). Participants initiated each trial with a spacebar press revealing a fixation point presented for 500–800 ms (duration drawn from a rectangular distribution). Next, a memory array that contained one or two colored circles presented on a large gray ring (8 of visual angle in diameter, 0.2° thick, 13.2 cd/m<sup>2</sup>) appeared for 250 ms. The center of the gray ring was 6° of visual angle to the left of fixation; thus, stimuli were presented between 2° and 10° to the left of fixation. On one-item trials, the stimulus was blue (0.4° in diameter, 71.0 cd/m<sup>2</sup>) or green (0.4° in diameter, 114 cd/m<sup>2</sup>), and on two-item trials, one stimulus was blue and the other was green. The memory array was followed by a 1,000-ms delay period with only the fixation point on the screen. After the delay period, the fixation point turned blue or green to indicate which stimulus to report. At the same time, a gray circular cursor (0.2° of visual angle in diameter, 13.2 cd/m<sup>2</sup>) appeared at the center of a gray ring (8° of visual angle in diameter, 0.2° thick, 13.2 cd/m<sup>2</sup>), and participants reported the remembered location of the probed stimulus by using the mouse to click on the perimeter of the probe ring.

Participants were instructed to remember the position of each sample stimulus on the gray ring as precisely as possible. To encourage participants to respond as accurately as possible, they received feedback with their average response error every 64 trials. Participants performed as many trials as they could complete during the 4-h EEG session, up to a maximum of 12 blocks of 128 trials each. Participants completed a short series of practice trials before starting the main experiment to verify that they understood the task. The number of to-be-remembered items (1 or 2) and the color of the probed item (green or blue) for each trial were counterbalanced across each block so that an equal number of each combination of trial types occurred in each block. The order of trial types was randomized for each block.

The angular position of each stimulus around the circular stimulus space was sampled from eight position bins, each spanning a 45° wedge of angular positions around the center of the sample space (bins were centered at 0°, 45°, and so forth, see Fig. 5A), with jitter added in 1° increments with a range of ±22° per bin to cover all 360° of possible locations to minimize categorical coding of stimulus location. On two-item trials, the position bins that each stimulus occupied were fully counterbalanced across trials for each observer

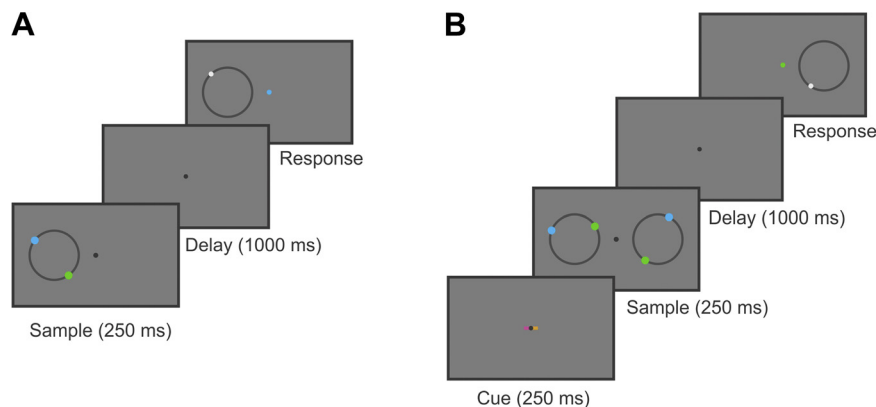


**Figure 1.** Task schematic for *experiments 1* and *2*. In both tasks, observers saw a brief sample display (250 ms) that contained to-be-remembered colored dots (1 or 2). After a brief delay (1,000 ms), the color of the fixation dot turned blue or green to indicate which item should be reported. Participants reported the angular position of the cued dot by mouse click on the perimeter of a ring. *A*: example two-item trial for *experiment 1*, which included only target items presented to the left of fixation. *B*: example two-item trial for *experiment 2*. At the start of each trial, participants were centrally cued (250 ms) to remember the location of items on the left or right while ignoring distractor items presented on the opposite side of fixation. Cues were 100% valid and the color indicating the target side (orange or magenta) was randomly assigned to each participant and consistent throughout the experiment.

(i.e., for a probed item in any given bin, the unprobed item appeared in each of the 8 possible bins equally often). Thus, the position bin that each stimulus occupied was random with respect to the other, which allowed reconstruction of spatial response functions (SRFs) for each stimulus independently. When both stimuli occupied the same position bin, their exact position within the bin was constrained so that the two items were separated by at least  $0.4^\circ$  of visual angle.

### Experiment 2 task procedure and stimuli.

Participants performed essentially the same lateralized memory task performed in *experiment 1*. On each trial, observers were centrally cued to remember the location of dots (1 or 2) presented to the left or right of fixation while ignoring the location of distractor dots presented on the uncued side of the screen (Fig. 1B).

Participants initiated each trial with a mouse click at fixation revealing a fixation point presented for 500–800 ms (randomly drawn as in *experiment 1*). Next, a cue appeared to indicate the target side of the array, that is, the cue was 100% valid in indicating the target side of the array. The cue consisted of a magenta ( $0.1^\circ \times 0.3^\circ$ ,  $65.9 \text{ cd/m}^2$ ) and orange ( $0.1^\circ \times 0.3^\circ$ ,  $69.7 \text{ cd/m}^2$ ) bar presented to either side of fixation. The color orange or magenta pointing to the target side of the screen was consistent throughout the experiment and was pseudorandomized across subjects so an equal number of subjects were assigned to each color mapping. Next, a memory array that contained one or two colored target circles presented to one side of fixation on a large gray ring ( $8^\circ$  of visual angle in diameter,  $0.2^\circ$  thick,  $13.2 \text{ cd/m}^2$ ) and the same number of colored distractor circles presented on a large gray ring on the opposite side of fixation appeared for 250 ms. The center of each gray ring was  $6^\circ$  of visual angle from fixation; thus, targets and distractors were presented between  $2^\circ$  and  $10^\circ$  from fixation. On one-item trials, the target stimulus was blue ( $0.4^\circ$  in diameter,  $69.3 \text{ cd/m}^2$ ) or green ( $0.4^\circ$  in diameter,  $68.5 \text{ cd/m}^2$ ) along with either a blue or green distractor (i.e., the distractor color was random with respect to the target color). On two-item trials, one target stimulus was blue and the other was green. The distractor array for two-item trials also contained one blue and one green stimulus. The memory array was followed by a 1,000-ms delay period with only the fixation point on the screen. After the delay period, the fixation point turned blue or green to indicate which stimulus to report. At the same time a gray circular cursor ( $0.2^\circ$  of visual angle in diameter,  $13.2 \text{ cd/m}^2$ ) appeared at the center of a gray ring ( $8^\circ$  of visual angle in diameter,  $0.2^\circ$  thick,  $13.2 \text{ cd/m}^2$ ) on the target side of the display, and participants reported the remembered location of the probed stimulus by using the mouse to click on the perimeter of the probe ring.

Participants were instructed that stimuli on the distractor side of the display would never be tested and to remember the position of each target stimulus on the gray ring as precisely as possible. To encourage participants to respond as accurately as possible while keeping their eyes on fixation, they received feedback with their average angular performance and number of trials rejected for blinks and eye movements every 72 trials. Participants performed as many trials as they could complete during the 4-h EEG session, up to a maximum of 13 blocks of 144 trials each. Set size (1 or 2),

probe color (green or blue), and target side (left or right) were counterbalanced across each block so that an equal number of each combination of trial types occurred in each block. The order of trial types was randomized for each block.

The angular position of each stimulus around the circular stimulus space was sampled from six position bins, each spanning a  $60^\circ$  wedge of angular positions around the center of the sample space (bins were centered at  $0^\circ$ ,  $60^\circ$ , and so forth, see Fig. 8A), with jitter added in  $1^\circ$  increments with a range of  $\pm 29^\circ$  per bin to minimize categorical coding of stimulus location. The number of bins was reduced from *experiment 1* (when we designed the task for *experiment 2*) to allow for efficient counterbalancing of target and distractor positions. On two-item trials, the position bins that each target stimulus occupied were fully counterbalanced across trials for each observer (i.e., for a probed item in any given bin, the unprobed item appeared in each of the 6 possible bins equally often). Thus, the position bin that each target stimulus occupied was random with respect to the other, which allowed reconstruction of spatial response functions (SRFs) for each target stimulus independently. The position bins of distractor stimuli relative to each other were counterbalanced on two-item trials as well. It was not possible to fully counterbalance the position of target and distractor stimuli relative to each other, however target and distractor position bins were random with respect to each other across trials, which allows for independent reconstruction of target and distractor stimuli. When both target stimuli occupied the same position bin, their exact position within the bin was constrained so that the two items were separated by at least  $0.4^\circ$  of visual angle. This distance requirement was not applied to distractors during the task, but was enforced at analysis by dropping all trials in which two-item distractors appeared within  $0.4^\circ$  of visual angle from each other ( $\sim 50$  trials per subject).

### Electrophysiology

The EEG was recorded from 32 active Ag/AgCl electrodes mounted in an elastic cap (Brain Products actiCHamp, Munich, Germany). The International 10–20 sites we recorded from were O2, Oz, O1, P8, P4, Pz, P3, P7, PO8, PO4, POz, PO3, PO7, T8, C4, Cz, C3, T7, FC6, FC5, F8, F4, Fp1, Fz, Fp2, F3, and F7. We attached two additional electrodes with stickers to the left and right mastoids and placed a ground electrode in the cap at position FPz. We used a right mastoid reference during data collection, and then referenced to the algebraic average of the left and right mastoids offline. EEG data were baseline corrected over the 300 ms before stimulus onset (*experiment 1*) and the 300 ms before cue onset (*experiment 2*). We recorded the electrooculogram (EOG) with four active electrodes, which we used to monitor for eye movements and blinks. We recorded horizontal EOG from a bipolar pair of electrodes affixed  $\sim 1$  cm from the external canthus of each eye, and we recorded vertical EOG from a bipolar pair of electrodes affixed above and below the right eye. We digitized data at 500 Hz using Brain Vision Recorder (Brain Products, Munich, German) running on a PC and filtered data offline (low cutoff = 0.01 Hz, high cutoff = 80 Hz, slope from low to high cutoff = 12 dB/octave). We kept impedance values below 10 k $\Omega$ .

## Eye Tracking

Gaze position was monitored using a desk-mounted Eye Link 1000 Plus infrared eye-tracking camera (SR Research, Ontario, Canada) while head location was stabilized with a chin rest. Useable eye-tracking data were obtained for 17 of 21 participants in *experiment 1* and 25 of 26 participants in *experiment 2*. In *experiment 1*, gaze data were inspected offline for ocular artifacts to aid in artifact rejection. In *experiment 2*, gaze data were used to reject trials in real time in order provide participants with online feedback about eye movements. Gaze data were also inspected for subtle eye movements offline to aid in artifact rejection.

## Artifact Rejection

Segmented EEG data were first subjected to an automatic artifact rejection pipeline to flag artifacts in the EEG signal (amplifier saturation, excessive muscle noise, and skin potentials). For *experiment 1*, EEG segments were from 300 ms before sample onset to 1,250 ms after sample onset, and for *experiment 2* segments were from 300 ms before cue onset to 1,250 ms after sample onset. Electrooculogram (EOG) and gaze data were also subjected to an automatic artifact rejection routine to flag ocular artifacts (blinks and eye movements  $> 0.5^\circ$  of visual angle). The EEG, EOG, and gaze data were then visually inspected for artifacts that the automatic rejection pipeline missed. Trials contaminated by artifacts were discarded. We discarded electrodes Fp1, Fp2, T7, and T8 for all observers because these channels contained excessive high-frequency noise for many participants. Data from one or two additional electrodes were discarded for three participants in *experiment 2* because of excessive high-frequency noise or sudden steps in voltage that occur when an electrode is damaged. The discarded electrodes for each participant were as follows: F7; F7 and F8; and FC5. For the analysis of gaze position, we further excluded trials in which the eye tracker was unable to detect the pupil, operationalized as any trial in which the horizontal gaze position was more than  $15^\circ$  from fixation or the vertical gaze position was more than  $8.5^\circ$  from fixation (off the computer monitor). A software error with the eye tracker caused it to periodically stop recording slightly early (up to 6 ms before the end of the delay period), thus we limited our gaze position analysis to time points when we have data for all trials and subjects.

Rejection of ocular artifacts was effective in that the maximum variation in grand average horizontal electrooculogram waveforms by target location bin was  $< 2 \mu\text{V}$  for all conditions in both experiments. Maximum variation in grand average vertical electrooculogram waveforms by target bin was  $< 3.5 \mu\text{V}$  for all conditions in both experiments. Thus eye movements in both experiments corresponded to variations in eye position of  $< 0.25^\circ$  of visual angle, or just slightly larger than the size of the fixation dot (33). For comparison, variation in grand-average horizontal gaze position data by target location in any was  $< 0.12^\circ$  of visual angle for all conditions in both experiments, and variation in grand-average vertical gaze position by target location was  $< 0.11^\circ$  of visual angle for all conditions in both experiments.

## Time-Frequency Analysis

Power values at each electrode and time point were calculated using the filter Hilbert method. Baselined EEG data

were first band-pass filtered using a two-way least squares finite impulse response filter (EEGLAB function: “eegfilt.m”) to calculate frequency-specific activity at each electrode. Data were band-pass filtered from 8 Hz to 12 Hz for  $\alpha$ -band analyses. Next, a Hilbert transform (MATLAB Signal Processing Toolbox) was applied to obtain the complex analytic signal. Finally, instantaneous power was calculated by squaring the complex magnitude of the complex analytic signal. Note, that to avoid edge artifacts during our time window of interest (34), a longer trial epoch of 800 ms before stimulus (*experiment 1*) or cue (*experiment 2*) onset and 1,750 ms after stimulus onset (both experiments) was used for filtering and calculating instantaneous power. The extraneous time points were discarded before classification.

## Pattern Classification and Partitioning Data into Training and Test Sets

Pattern classification was conducted on the topographic distribution of  $\alpha$ -band power across electrodes. A naïve Bayes classifier implementation of a linear discriminant analysis was used to classify the probed position at each time point (the `classify.m` function in MATLAB with `diaglin` argument).

For the pattern classification procedure, artifact-free trials were first partitioned into independent sets of training and test data for each observer. Across all analyses, trials were partitioned into three independent sets. The number of trials for each set size, position bin, and (in *experiment 2* only) hemisphere in each set were equated. Because of this constraint, a subset of trials was not assigned to any set. Thus, an iterative approach was used to make use of all available trials. For each iteration, trials were randomly partitioned into sets, as described, and pattern classification was performed on the resulting training and test data. Therefore, the trials that were not included in any set were different for each iteration. The resulting classification outputs across iterations were averaged. This iterative approach reduced noise in the resulting classifier outputs by minimizing the influences of idiosyncrasies that were specific to any given assignment of trials to sets. One hundred iterations were conducted for all analyses.

Once trials were assigned to the three sets, averages for each position bin in each set were calculated to obtain a matrix of power values across all electrodes for each position bin (electrodes  $\times$  position bin), for each time point. A leave-one-out-cross-validation routine was used such that two of three sets served as training data and the remaining set served as the test data. The classifier routine was applied three times using each of the three matrices as the test set, and the remaining two as the training set.

For *experiment 1*, the classifier was always trained on an equal mixture of one- and two-item trials. Only the data included in the test set varied by analysis. We trained and tested the classifier in this manner whenever possible because it is difficult to interpret differences in selectivity between conditions if a different training set is used for each condition (35). For the combined one- and two-item analysis (Fig. 5B), the classifier was also tested on an equal mixture of one- and two-item trials. For analyses focused on one- and two-item trials separately (Fig. 4), the classifier was tested on one- and two-item data separately. In *experiment 2*, data

were partitioned into training and test sets as described for *experiment 1*, with the exception that classification was conducted on left and right targets separately.

To obtain spatial response functions (SRFs), classifier outputs for each position bin (i.e., Fig. 5B) were circularly shifted to a common center so the center position was the position corresponding to the probed stimulus (i.e., 0 on the target offset  $y$ -axis; Fig. 4A), these shifted spatial response functions were then averaged across all position bins to obtain an SRF. Confusion matrices for each condition were simply the unshifted classifier outputs for each position bin. In *experiment 2*, targets were presented in circular spaces to both the left and right of fixation. To obtain confusion matrices for model comparison that included both hemifields (all-item, one-item, and two-item comparisons), pattern classification outputs were averaged across matched positions relative to fixation for left and right trials.

Finally, because the exact patterns of  $\alpha$ -band activity that correspond to each remembered position likely vary across participants, we applied the pattern classification routine separately for each participant and statistical analyses were performed on the classifier output. This approach allowed us to disregard differences in how location-selective activity is mapped to scalp-distributed patterns of power across participants and instead focus on the profile of activity in the common stimulus or information space (36).

## Statistical Analysis

### Modeling response error.

Response error was measured as the number of degrees between the presented angular location on the target ring and the reported angular location on the target ring. Errors ranged from  $0^\circ$  (a perfect response) to  $\pm 180^\circ$  (a maximally imprecise response). To quantify memory performance, a mixture model was fit to the distribution of response errors for each participant using MemToolbox (37). The distribution of response errors for one-item trials was modeled as a two-component mixture mode, comprising a von Mises distribution centered on the correct value (i.e., a response error of 0), corresponding to trials in which the probed location was remembered, and a uniform distribution, corresponding to guesses in which the reported location was random with respect to the probed location. We obtained maximum likelihood estimates for two parameters: 1) the dispersion of the von Mises distribution (SD), which reflects response precision; and 2) the height of the uniform distribution ( $p_{\text{Guess}}$ ), which reflects the probability of guessing. For two-item trials, the distribution of response errors was modeled as a three-component mixture model that included an additional von Mises component centered on the location of the unprobed target item, corresponding to trials in which participants mistakenly reported the location of the unprobed target item ( $p_{\text{Swap}}$ ). Thus, maximum likelihood estimates were obtained for the same parameters as one-item trials (SD and  $p_{\text{Guess}}$ ), with the addition of a third parameter that reflects the probability of swaps ( $p_{\text{Swap}}$ ), that is the probability of reporting the other location that was shown in the target array.

### Spatial selectivity.

Linear regression was used to measure response function slope and quantify the spatial selectivity of response

functions. Specifically, the slope of the response function was calculated as a function of distance from the remembered location after collapsing across location bins equidistant from the remembered location (e.g.,  $\pm 2$  bins). Higher response function slope values indicate greater spatial selectivity.

### Model comparison.

For the polar angular model, we assumed that  $\alpha$ -band activity tracks the angular location of stimuli relative to fixation. We first calculated the squared distance  $(s - r)^2$  between the angular location (in degrees) relative to fixation of each possible location  $s$  and every possible stimulus location  $r$ . For the coordinate model, we assumed that  $\alpha$ -band activity tracks the Euclidean distance between stimuli, and we first calculated the squared Euclidean distance  $\left(\sqrt{(s_x - r_x)^2 + (s_y - r_y)^2}\right)^2$  between the  $x$  and  $y$  coordinates (in pixels, the maximum distance between any two points in the target space is 383 pixels) of each possible location  $s$  and every possible stimulus location  $r$ .

Next, for both models, we calculated the average squared distance between every location in each presented stimulus bin and every location in each possible classifier output bin to obtain a vector ( $\varphi$ ) of average squared distances between the locations in each presented stimulus bin relative to the locations in each classifier output bin. We then modeled the profile of expected classifier outputs for each presented stimulus location bin as follows:

$$f(\varphi) = b + e^{-(\varphi - \mu)/2\sigma^2},$$

where  $\varphi$  is a vector of distances (average squared distance between locations in the presented stimulus bin and locations in each classifier output bin) and  $\mu$  is the mean of a Gaussian normal distribution that is fixed at zero (centered on the distance from the presented stimulus bin),  $\sigma$  equals the standard deviation of the Gaussian normal distribution, and  $b$  equals the baseline of the function. We then converted the resulting tuning function for each presented location bin to a probability vector that sums to 1, by dividing each element in the tuning function by the sum of the tuning function

$$p(\text{classified}) = \frac{f(\varphi)}{\sum_{i=1}^n f(\varphi_i)},$$

to obtain an estimate of classifier outputs for each presented location bin for each parameterization of the model. Fitting of each model was performed via a grid search procedure in which we searched Gaussian values of 0.1 to 400 in steps of 0.1 and searched baseline values of 0.01 to 10 in steps of 0.01. The best fitting parameters were defined as those that minimized the residual sum of squared errors between the predicted classifier outputs and the actual classifier outputs for all presented locations. Thus, one set of best fitting parameter values was obtained for all presented locations.

The Bayesian information criterion [BIC; see Ref. 38 for a similar implementation (39)] was calculated to compare the goodness of fit of each model using the following equation:

$$\text{BIC} = k \ln(n) + n \ln\left(\frac{\text{RSS}}{n}\right),$$

where  $k$  is the number of model parameters,  $n$  is the number of data points being simultaneously fit, and RSS is the residual sum of squares. Lower (i.e., more negative) values of BIC indicate a better fit accounting for the number of parameters of the model.

**Cluster-based permutation test.**

A cluster-based permutation test was used to determine when spatial selectivity was reliably above chance while controlling for multiple comparisons (34, 40). Periods of above-chance spatial selectivity were identified for each analysis by performing a one-sided  $t$  test against a slope of 0 at each time point in the  $\alpha$ -band analyses. Next, clusters of contiguous time points that exceeded chance were identified. For each cluster, a test statistic was calculated by summing all the  $t$  values in the cluster. A Monte Carlo randomization procedure was used to empirically approximate a null distribution for this test statistic. Specifically, the pattern classification procedure for each analysis was repeated 1,000 times for each subject, but the bin labels within each training and test set were randomized. For each permutation of the randomization analysis, spatial selectivity was calculated across time to identify clusters of above-chance spatial selectivity using the same approach that was applied to the nonrandomized data. For each permutation, the highest summed test statistic for any cluster was calculated resulting in a null distribution of 1,000 cluster statistics. Finally, clusters that had test statistics larger than the 95th percentile of the null distribution were identified. Thus, the cluster test was a one-tailed test with an  $\alpha$  level of 0.05 corrected for multiple comparisons.

**Data Availability**

Data and analysis code for both experiments can be found on the Open Science Framework (<https://osf.io/t5n9z/>).

**RESULTS**

**Experiment 1**

*Experiment 1* was designed to determine whether  $\alpha$ -band activity tracks the vertical and horizontal coordinates of attended stimuli within a visual hemifield or if the resolution of  $\alpha$ -band activity is limited to tracking the angular coordinates of stimuli around fixation. We note here, that we made

the decision to present trials exclusively to the left visual hemifield in *experiment 1* for two reasons. First, given our uncertainty about whether or not  $\alpha$ -band power tracks the precise locations presented within a single hemifield in the first place, we sought to maximize the number of trials presented within each location bin rather than testing whether the results apply to presentation in both hemifields. Second, parietal networks are thought to play a critical role in the deployment of spatial attention (41, 42), and parietal and occipital networks are thought to be generators of  $\alpha$ -band activity (43, 44). There is a well-known asymmetry in parietal attention networks in which right parietal cortex primarily controls attention to the left side of space, whereas both the left and right hemispheres control attention to the right side of space (41, 45). Based on these known hemispheric asymmetries, we worried that it might be possible to decode locations presented to the right visual field but not the left visual field. Thus, we decided that presenting stimuli to the left visual field would be a more conservative approach for answering whether  $\alpha$ -band activity tracks fine grained-representations within a visual hemifield.

**Behavior.**

Observers' mnemonic precision (SD) was worse (Fig. 2A) when they maintained two items ( $M = 10.2^\circ$ ;  $SD = 2.3^\circ$ ) than when they maintained one item [ $M = 8.7^\circ$ ;  $SD = 2.3^\circ$ ;  $t(20) = 8.18$ ;  $P < 0.0001$ ]. We observed negligible guessing ( $p_{\text{Guess}}$ ; Fig. 2B) in both one-item ( $M = 0.44\%$ ;  $SD = 0.64\%$ ) and two-item trials ( $M = 0.33\%$ ;  $SD = 0.52\%$ ) and did not see a reliable difference in guess rate between conditions [ $t(20) = -1.005$ ;  $P = 0.327$ ]. Observers were unlikely to report the location of the unprobed item ( $p_{\text{Swap}}$ ; Fig. 2C) on two-item trials ( $M = 0.70\%$ ;  $SD = 1.06\%$ ). Finally, median response times (Fig. 2D) were slower for two-item trials ( $M = 1,344$  ms;  $SD = 442$  ms) than one-item trials [ $M = 1,225$  ms;  $SD = 419$  ms;  $t(20) = 12.22$ ;  $P < 0.0001$ ]. Thus, subjects' behavior was consistent with canonical findings in the literature, and we now turn to the main question of how  $\alpha$ -band activity tracks remembered locations.

**$\alpha$ -Band activity tracks fine-grained representations within a hemifield.**

To determine whether  $\alpha$ -band activity tracks fine-grained representations within a visual hemifield or is only sensitive to angular locations around fixation, we first looked at the topography of delay period  $\alpha$ -band power for each remembered position. Figure 3 shows the grand average scalp distribution of percent change in delay period  $\alpha$ -band power (250–1,250

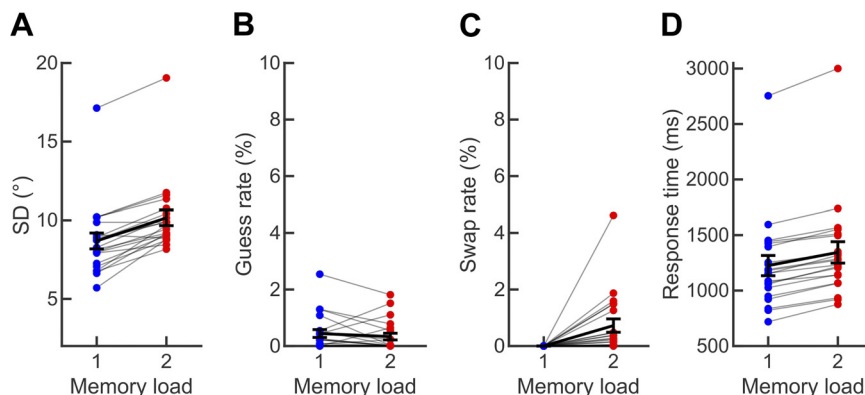


**Figure 2.** Behavioral performance for *experiment 1*. Showing mixture model parameters for mnemonic precision (SD) (A), guess rate ( $p_{\text{Guess}}$ ) (B), the rate of reporting the unprobed item instead of the probed item ( $p_{\text{Swap}}$ ) (C), and median response times as a function of memory load (1 vs. 2 items) (D). Note that swap rate was not defined for one-item trials and is plotted at zero for all participants. Light gray lines represent individual participants. Black lines represent the mean. Error bars represent  $\pm 1$  SE.

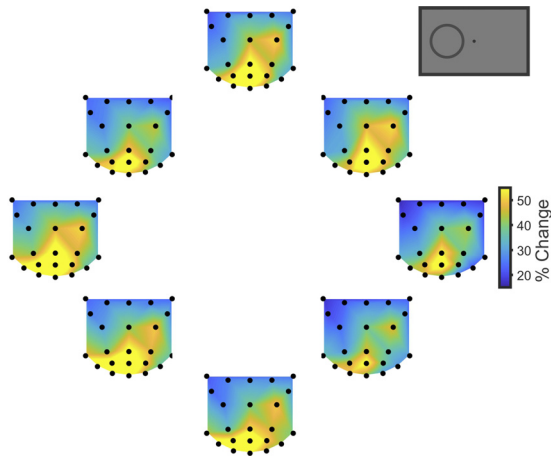


**Figure 3.** Topography of  $\alpha$ -band power during the memory delay (250–1,250 ms) of *experiment 1*. Topography of percent change in  $\alpha$ -band power for each remembered position relative to the topography of baseline  $\alpha$ -band power (–300 to –100 ms).

ms) relative to baseline as a function of remembered location. We used a baseline of –300 to –100 ms before sample onset to avoid including  $\alpha$ -band activity related to the sample via temporal smearing that is inherent to the filtering process (34). These scalp maps reveal that the pattern of  $\alpha$ -band power across electrodes subtly varies as a function of the remembered location within a hemifield, which extends on previous work showing that the topography of  $\alpha$ -band power varies with angular location around fixation (8, 46). Note that we plotted these patterns relative to the pretrial baseline to facilitate comparison with past work that employed the same method for stimuli presented around fixation, whereas the  $\alpha$ -band power used for pattern classification was not baseline corrected. Thus, these analyses are complementary ways of analyzing the same underlying signal.

To test whether topographic patterns of  $\alpha$ -band activity (8–12 Hz) contain sufficient information to reliably track remembered locations moment-by-moment throughout the task, we used a linear discriminant classifier to decode the location of remembered stimuli from patterns of  $\alpha$ -band power at each time point during the memory task. We observed robust spatial response functions for both one-item (Fig. 4A) and two-item (Fig. 4B) trials, with both conditions showing peak classification in the remembered location (a target offset of 0) during the working memory delay period. Next, we quantified spatial selectivity across time for each condition by calculating the slope of the SRF at each time point (see METHODS). Cluster-based permutation tests revealed that the spatial selectivity of  $\alpha$ -band SRFs was reliably above 0 from shortly after the sample onset to the end of the delay period for one-item trials, and reliably above zero from shortly after sample onset through the first second of the delay period for two-item trials ( $P < 0.05$ ; corrected for multiple comparisons; Fig. 4C).

**$\alpha$ -Band representations reflect the vertical and horizontal coordinates of remembered locations.**

Our observation of reliable spatially selective  $\alpha$ -band activity provides evidence that  $\alpha$ -band activity tracks the encoding

and maintenance of the location of items presented within a visual hemifield. However, this observation alone does not provide enough information to determine whether  $\alpha$ -band activity tracks both the horizontal and vertical coordinates of a remembered stimulus relative to fixation or whether  $\alpha$ -band activity only tracks the angular coordinates of a stimulus around fixation. To distinguish between these possibilities, we ran a linear discriminant analysis on data from both conditions to maximize the number of trials included in each position bin and then examined the average confusion matrix of classifier outputs (i.e., the proportion of classifier responses in each spatial bin for each remembered location) during the working memory delay period (Fig. 5B). If  $\alpha$ -band activity is sensitive to both the vertical and horizontal coordinates of the stimulus, we expected to observe robust spatial selectivity for each remembered location. Alternatively, if  $\alpha$ -band activity is sensitive to the angular location of stimuli relative to fixation, we instead expected to observe robust SRFs at the extremes of the vertical axis (e.g., stimuli in bins 3 and 7, see Fig. 5, A and C) and weak double peaked SRFs for positions along the midline. Supporting the hypothesis that  $\alpha$ -band activity tracks both the vertical and horizontal coordinates of a stimulus relative to fixation, we observed a clear graded SRF for each of the eight position bins and little evidence of confusion between midline positions (e.g., 1 and 5; Fig. 5B). Next, we conducted a

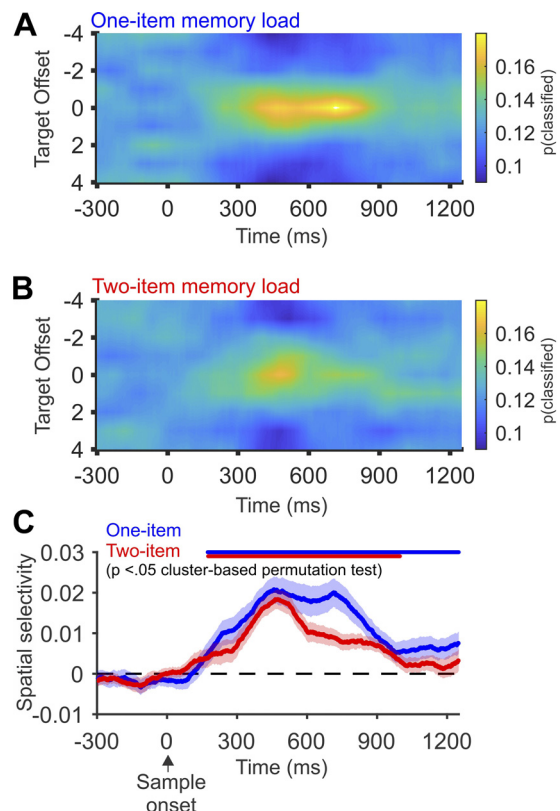


**Figure 4.**  $\alpha$ -Band spatial response functions as a function of memory load for *experiment 1*. Average  $\alpha$ -band spatial response functions for the one-item (A) and two-item (B) conditions. C: the spatial selectivity of spatial response functions across time (measured as response function slope, see METHODS) as a function of memory load. The blue (one-item) and red (two-item) markers at the top of the panel indicate the period of above-chance selectivity obtained using a cluster-based permutation test. The shaded error bars reflect  $\pm 1$  SE across observers.

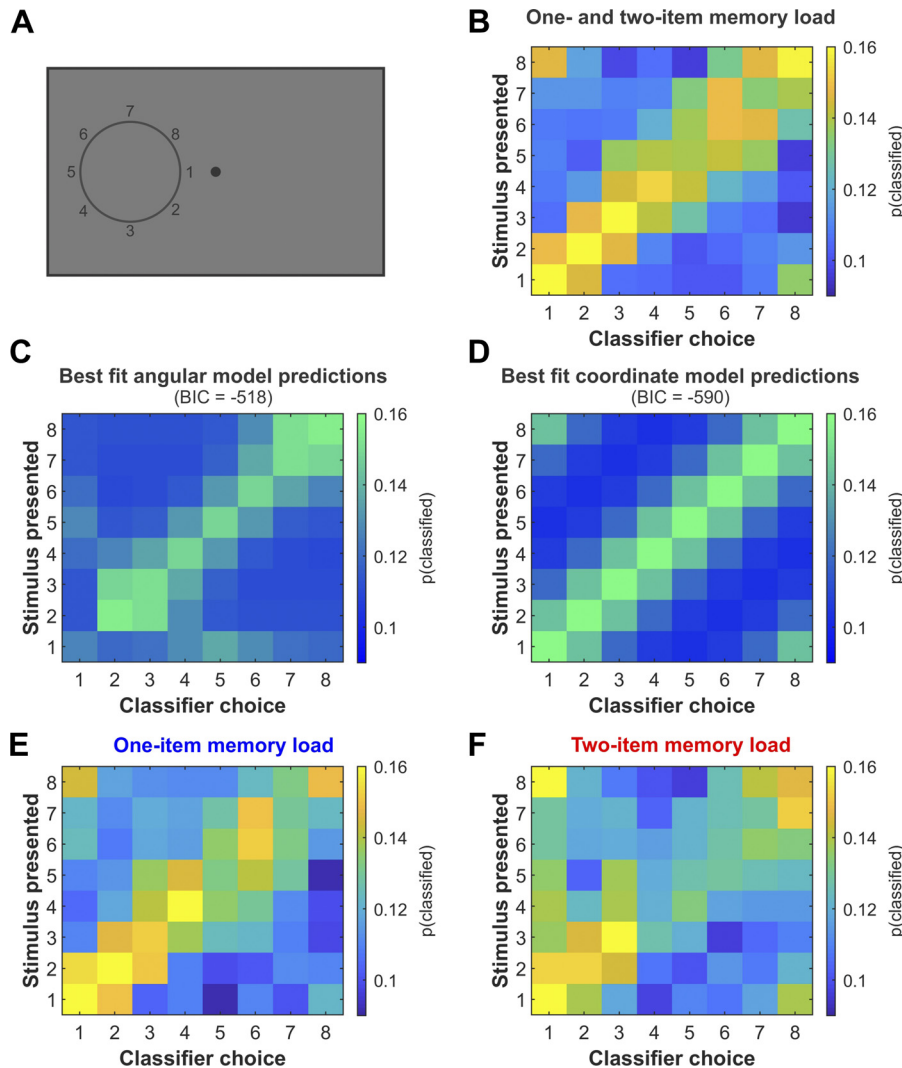


**Figure 5.** Unshifted classifier outputs from  $\alpha$ -band power during the memory delay (250–1,250 ms) of *experiment 1*. *A*: sample stimuli varied in position around the response space and were categorized as belonging to one of eight position bins (each a 45° wedge of the stimulus space) centered on bin 1, 2, etc. *B*: confusion matrix of classifier choices for one- and two-item stimuli. *C*: confusion matrix of best fit angular model to the one- and two-item confusion matrix. *D*: confusion matrix of best fit coordinate model to the one- and two-item confusion matrix. *E*: confusion matrix of classifier choices for one-item stimuli. *F*: confusion matrix of classifier choices for two-item stimuli. The coordinate model provides a better fit (lower BIC score) of the observed data, indicating that the topography of  $\alpha$ -band activity tracks the precise vertical and horizontal coordinates of remembered stimuli and not just angular location relative to fixation. BIC, Bayesian information criterion.

model comparison on the average confusion matrix to test whether the model predicted by the polar angle of stimuli relative to fixation or the two-dimensional coordinates of stimuli relative to fixation provided the best fit of the observed data. We found that the best fitting coordinate model (Fig. 5D) provided a better fit of the data after accounting for the number of sample points than the best fitting angular model (Fig. 5C; Table 1). In line with past work demonstrating that spatial  $\alpha$ -band representations (13), we observed a similar pattern of results when the average classifier output for each position was examined separately for the one-item (Fig. 5E) and two-item (Fig. 5F) trials. The coordinate model provided a better fit of the data than the angular model for both set sizes (Table 1). As a general guideline, a difference in BIC scores of 2–6 is taken

as positive evidence that there is a difference between two model fits, a difference of 6–10 is interpreted as strong evidence, and a difference of more than 10 is interpreted as very strong evidence (47). Thus, the difference in BIC scores we observed here (all  $\Delta$ BICs > 20) can be interpreted as very strong evidence in favor of the coordinate model.

**Discussion.**

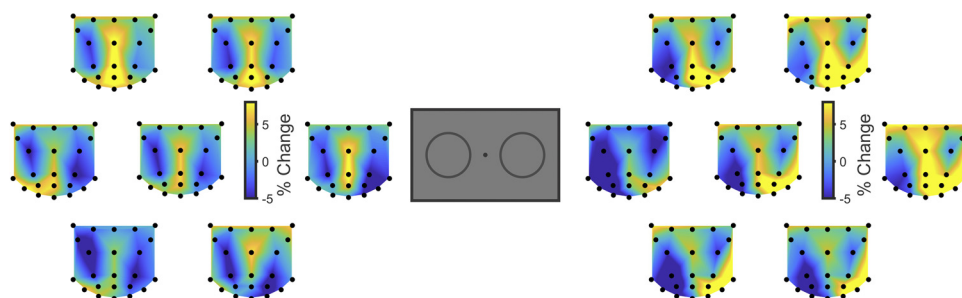
In *experiment 1*, we found that  $\alpha$ -band activity tracks the vertical and horizontal coordinates of remembered stimuli when stimuli were consistently presented to the same side of fixation in the absence of distractors. Although a strength of the design in *experiment 1* was that it allowed us to maximize the number of trials presented in each position bin, covert

**Table 1.** Comparison of model fits for *experiment 1*

Trial Type	<i>b</i> Ang	<i>b</i> Coord	$\sigma$ Ang	$\sigma$ Coord	RSS Ang	RSS Coord	BIC Ang	BIC Coord	$\Delta$ BIC
All	2.63	1.28	16.6	200.8	0.0173	0.0056	-517.66	-589.63	71.97
One item	3.48	1.82	15.9	166.1	0.0200	0.0092	-508.13	-558.09	49.96
Two items	4.73	1.85	13.2	249.4	0.0140	0.0092	-530.92	-557.72	26.80

Ang, angular model; BIC, Bayesian information criterion; Coord, coordinate model; RSS, residual sum of squares.

**Figure 6.** Topography of  $\alpha$ -band power during the memory delay (250–1,250 ms) of *experiment 2*. Topography of percent change in  $\alpha$ -band power for each remembered position relative to the topography of baseline  $\alpha$ -band power (–300 to –100 ms before the hemifield cue). The scalp topographies in the center of each circular space show the topography of all target positions within a hemifield relative to baseline.



attention typically has to operate flexibly by selecting information across the entire visual field, often in the presence of distractors. Thus, it is possible that the results from *experiment 1* represent an upper bound on the resolution of spatially specific  $\alpha$ -band activity, whereas the resolution of this spatially specific  $\alpha$ -band activity is considerably worse in more traditional memory tasks in which the target hemifield changes trial-to-trial and targets are accompanied by distractors. Our goal in *experiment 2* was to test whether the spatial selectivity we observed in *experiment 1* is also present in a more traditional lateralized design.

### Experiment 2

In *experiment 2*, we extend our observations from *experiment 1* and show that the precise coordinates of remembered stimuli could be decoded when targets were presented to either side of fixation in the presence of an equal number of distractors in the opposite hemifield.

#### ***α*-Band activity tracks fine-grained representations in both the left and right hemifields.**

In *experiment 1*, we provided evidence that  $\alpha$ -band activity tracks the coordinates of remembered stimuli when targets were presented to the left of fixation. In *experiment 2*, we tested whether the spatial selectivity of  $\alpha$ -band representations varied as a function of whether target stimuli were presented to the left or right visual hemifield. **Figure 6** shows the grand average scalp distribution of percent change in delay period  $\alpha$ -band power (250–1,250 ms) relative to baseline (–300 ms to –100 ms before the hemifield cue) as a function of remembered location. As in *experiment 1*, these scalp maps show that the pattern of  $\alpha$ -band power across electrodes varies as a function of remembered location within each hemifield.

Consistent with the results from *experiment 1*, linear discriminant classification revealed robust decoding of remembered locations when stimuli were presented in the left visual hemifield (**Fig. 7A**). We also found that we obtained robust decoding of remembered stimuli for items presented to the right hemifield (**Fig. 7B**). We did not observe a difference in spatial selectivity for targets presented to the left ( $M = 0.0114$ ,  $SD = 0.0156$ ) and right ( $M = 0.0126$ ,  $SD = 0.0114$ ) visual field [ $t(25) = -0.3867$ ,  $P = 0.702$ ; **Fig. 7C**]. These results show that patterns of  $\alpha$ -band activity can be used to track the

location of stimuli presented to either visual hemifield in the presence of distractors in the opposite hemifield.

Our motivation for using only the left visual field in *experiment 1* was because of the well-known asymmetry in visual parietal attention networks in which right parietal cortex primarily controls attention to the left side of space, whereas parietal cortex in both the left and right hemispheres control attention to the right side of space (41, 45). Although we found robust decoding of remembered

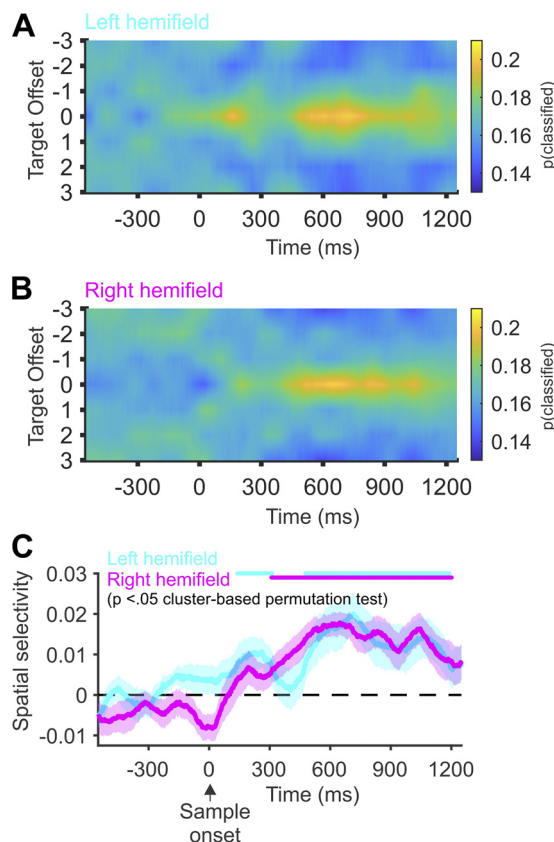


**Figure 7.**  $\alpha$ -Band spatial response functions as a function of target hemifield for *experiment 2*. Average  $\alpha$ -band spatial response functions for targets presented to the left (A) and right (B) hemifields. C: the spatial selectivity of spatial response functions across time (measured as response function slope, see METHODS) as a function of target hemifield. The cyan (left hemifield) and magenta (right hemifield) markers at the top of the panel indicate the period of above-chance selectivity obtained using a cluster-based permutation test. The shaded error bars reflect  $\pm 1$  SE across observers.

locations presented to the left visual field in both experiments, we wondered if there might be asymmetries in the decoding accuracy for stimuli presented to the left versus right hemifield if we focused our analysis on lateralized subsets of electrodes. For example, one might expect to observe superior spatial selectivity from electrodes on the right side of the cap relative to electrodes on left side of the cap for stimuli presented to the left visual hemifield and no difference in selectivity across electrodes for stimuli presented to the right visual hemifield.

To test this question, we ran a classifier analysis using only electrodes on the right side of the cap (“O2,” “PO4,” “PO8,” “P4,” “P8,” “C4,” “FC6,” “F8,” “F4”) or left side of the cap (“O1,” “PO3,” “PO7,” “P3,” “P7,” “C3,” “FC5,” “F7,” “F3”). For *experiment 2*, we examined the average delay period selectivity with a two-way repeated-measures ANOVA (with factors for visual hemifield and electrode side). This revealed a significant main effect of electrode side [ $F(1,25) = 7.39, P = 0.012$ ] such that spatial selectivity was higher for right electrodes ( $M = 0.0111, SD = 0.011$ ) than left electrodes ( $M = 0.0065, SD = 0.01$ ) regardless of the presented hemifield. We did not observe a significant main effect of visual hemifield [ $F(1,25) = 0.113, P = 0.739$ ] and the factors of visual hemifield and electrode side did not interact significantly [ $F(1,25) = 1.486, P = 0.234$ ]. However, we did not observe a significant difference in spatial selectivity between left ( $M = 0.0108, SD = 0.0087$ ) and right ( $M = 0.0093, SD = 0.009$ ) electrodes in *experiment 1* [ $t(20) = 0.65, P = 0.523$ ] in contrast to the results from *experiment 2*. Thus, although it is possible that the randomized hemifield of target stimuli or presence of distractor items in *experiment 2* are important for generating this effect, we will not focus further on this observation.

### ***$\alpha$ -Band representations track the vertical and horizontal coordinates of stimuli in both the left and right hemifields.***

As in *experiment 1*, our goal was to determine whether  $\alpha$ -band activity tracks both the horizontal and vertical coordinates of remembered stimuli or whether  $\alpha$ -band activity only tracks the angular coordinates of stimuli relative to fixation. We ran a linear discriminant analysis on data, including each hemifield and set size, and then examined the average confusion matrix of classifier outputs (i.e., the proportion of classifier responses in each spatial bin for each remembered location) during the working memory delay period (Fig. 8B). If  $\alpha$ -band activity is sensitive to both the vertical and horizontal coordinates of the stimulus, we expected to observe robust spatial selectivity for each remembered location with confusions bleeding only into neighboring locations on the presentation ring (Fig. 8D) while we expected a pattern of confusions among items presented along the midline if  $\alpha$ -band activity is limited to tracking the angular location of remembered items (Fig. 8C). In line with our results from *experiment 1* and the hypothesis that  $\alpha$ -band activity tracks both the vertical and horizontal coordinates of remembered

stimuli, we observed a clear graded SRF for each of the six possible position bins when averaging across matched position bins for left and right targets (Fig. 8B). To formally test this observation, we conducted a model comparison to determine whether the model predicted by the angular location of stimuli relative to fixation or the two-dimensional coordinates of stimuli provided the best fit of the observed data. We found that the best fitting coordinate model (Fig. 8D) provided a better fit of the data after accounting for the number of sample points and model parameters than the best fitting angular model (Fig. 8C; Table 2). We observed a similar pattern of results in which the coordinate model provided a better fit of the data when the average classifier output for each position was examined separately for left (Fig. 8E) and right (Fig. 8F) trials (Table 2). As in *experiment 1*, we also observed a similar pattern of results when the average classifier output for each position was examined separately for one-item (Fig. 8G) and two-item (Fig. 8H) trials. With the coordinate model providing a better fit of the data than the angular model for all trial types (Table 2). BIC differences ranged from 7.8 to 27.8, providing strong to very strong evidence in favor of the coordinate model (47).<sup>1</sup>

## **DISCUSSION**

Covert spatial attention is proposed to play a critical role in how we sample available visual information and in how we maintain (3–5) and retrieve memories (48, 49). Thus, there is great interest in characterizing and understanding neural signals that track the moment-by-moment focus of covert attention. Recent work has proposed that EEG  $\alpha$ -band activity is one such signal that tracks the focus of covert attention (1, 2). In line with this view is a substantial body of work showing that EEG  $\alpha$ -band activity tracks the angular position of attended (6–9) and remembered locations (10–14). However, a defining feature of spatial attention is that it facilitates processing in a specific region of the visual field (15, 17), and extant work has yet to determine whether  $\alpha$ -band activity can track the two-dimensional coordinates of attended or remembered stimuli.

In the current study, we tested whether EEG  $\alpha$ -band activity reflects the focus of covert attention in lower level visual areas with spatially precise receptive fields with resolution sufficient to track the two-dimensional coordinates of remembered stimuli within a visual hemifield or if instead  $\alpha$ -band activity reflects the effects of covert spatial attention at a coarser level of visual processing in attentional control regions with large visual fields (such as the frontal eye field) and is limited to tracking the angular coordinates of remembered stimuli. Our results show that patterns of EEG  $\alpha$ -band activity can be used to track the location of one or two remembered items throughout the delay period of a lateralized working memory task. Critically, model comparison revealed that these same patterns of  $\alpha$ -band activity reflect the two-dimensional coordinates of remembered stimuli rather than their angular location relative to fixation. Together these results provide evidence that  $\alpha$ -band activity

<sup>1</sup>We note that our analysis of *experiment 2* is limited to extending the critical finding of *experiment 1*, that  $\alpha$ -band activity tracks the coordinates of target stimuli rather than their angular location relative to fixation.

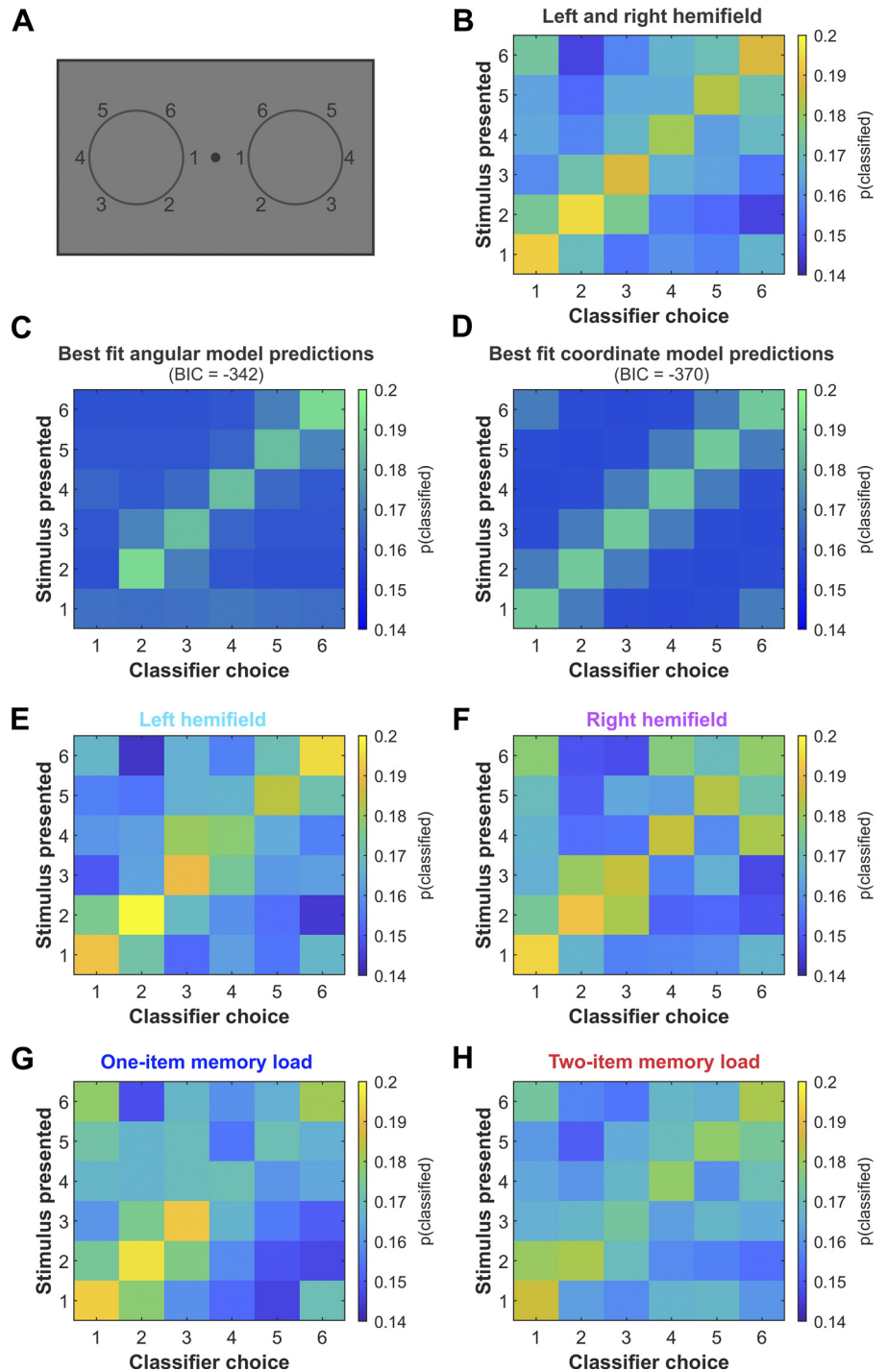


**Figure 8.** Unshifted classifier outputs from  $\alpha$ -band power during the memory delay (250–1,250 ms) of *experiment 2*. *A*: sample stimuli varied in position around the response space and were categorized as belonging to one of six position bins in each target hemifield (each a 60° wedge of the stimulus space) centered at bin 1, 2, etc. *B*: average delay period confusion matrix of classifier choices for all trial types. *C*: confusion matrix of best fit angular model to the all trial type confusion matrix. *D*: confusion matrix of best fit coordinate model to the all trial type confusion matrix. *E*: confusion matrix of classifier choices for stimuli presented to the left hemifield. *F*: confusion matrix of classifier choices for stimuli presented to the right hemifield. *G*: confusion matrix of classifier choices for one-item stimuli. *H*: confusion matrix of classifier choices for two-item stimuli. The coordinate model provides a better fit (lower BIC score) of the observed data for all categories of stimuli, indicating that the topography of  $\alpha$ -band activity tracks the precise vertical and horizontal coordinates of remembered stimuli and not just angular location relative to fixation. BIC, Bayesian information criterion.

tracks the spotlight of covert attention focused on locations being maintained in working memory.

At least one previous study has found that  $\alpha$ -band power does not track the eccentricity of attended locations (29). How do we reconcile the present findings with this work? One possibility is that the sensitivity of the topography of  $\alpha$ -band power to differences in eccentricity is fairly coarse in the absence of differences in angular location. For example, Roijndijk et al. (29) used stimuli that were 3.5° of visual angle in eccentricity. In the current experiment, stimuli within a hemifield that

varied only in eccentricity, and not angular location, were separated by 8° of visual angle. Thus, our observation that we could clearly differentiate stimuli along the midline is in line with the past observation that patterns of  $\alpha$ -band activity could differentiate eccentricity along the midline when stimuli are more than 6° of visual angle apart (28). Interestingly, based only on past work, we might have predicted that it would not be possible to distinguish between the patterns of  $\alpha$ -band activity for positions that were quite similar in visual angle (i.e., bins 2 and 3; Fig. 4) and much closer in eccentricity

**Table 2.** Comparison of model fits for experiment 2

Trial Type	<i>b</i> Ang	<i>b</i> Coord	$\sigma$ Ang	$\sigma$ Coord	RSS Ang	RSS Coord	BIC Ang	BIC Coord	$\Delta$ BIC
All	4.94	4.19	11.9	138.8	0.0022	0.0010	-342.3	-370.1	27.8
Left	4.34	3.77	11.1	138.4	0.0027	0.0013	-334.7	-360.8	26.1
Right	1.90	4.70	62.9	139.6	0.0035	0.0028	-325.8	-333.5	7.8
One item	6.09	5.03	9.9	147.6	0.0037	0.0025	-323.6	-337.4	13.8
Two items	5.17	6.89	48.2	128.6	0.0015	0.0011	-354.8	-367.9	13.2

Ang, angular model; BIC, Bayesian information criterion; Coord, coordinate model; RSS, residual sum of squares.

( $\sim 2^\circ$  of visual angle apart). However, we observed a clear peak in classifier responses at each of these positions, suggesting that a combination of differences in eccentricity and angular location may be easier to differentiate than eccentricity differences alone. Across both experiments, we found that patterns of EEG  $\alpha$ -band activity at adjacent locations were more similar than patterns at more distant locations. This graded pattern of location selectivity is in line with past observations tracking angular locations with  $\alpha$ -band activity (11, 13). Furthermore, this observation provides a potential explanation for a recent observation that patterns of  $\alpha$ -band activity that track remembered angular locations at one eccentricity can be used to reconstruct the focus of spatial attention at the same angular location at a different eccentricity [see Fig. 6 of van Moorselaar et al. (9)]. Specifically, it seems plausible that the patterns of  $\alpha$ -band activity tracking stimuli at different eccentricities and the same angular location are similar enough to allow generalization, even if the patterns of  $\alpha$ -band activity observed at different eccentricities are not identical.

fMRI work has shown that spatial priority maps throughout the visual hierarchy reflect the focus of covert attention and that representation size in these priority maps increases from early to later visual areas (26, 50). The present findings indicate that the receptive field sizes of the neurons in the area or areas generating this  $\alpha$  activity are of small to moderate size (18). Our findings are in line with recent magnetoencephalography (MEG) source localization work finding that  $\alpha$  sources for stimuli presented around fixation approximate the retinotopic organization of early- to mid-level visual areas (24) and suggest that both EEG and MEG activity may reflect similar underlying sources. However, the spatial coverage of the present work was fairly sparse, so exactly which level or levels of the visual processing stream that these spatially specific patterns of  $\alpha$ -band activity reflect remains an open question. Future experiments employing a more fine-grained distribution of target stimuli may prove a useful means of determining the resolution of  $\alpha$ -band activity and identifying precisely which areas of the visual hierarchy these spatially specific  $\alpha$ -band representations reflect.

Throughout the manuscript, we have argued that patterns of EEG  $\alpha$ -band activity on the scalp reflect a spotlight of spatial attention to locations maintained in working memory. Although our results clearly show that patterns of  $\alpha$ -band activity reflect the specific two-dimensional coordinates of target stimuli, we think it is worth noting that long-standing questions about the extent to which spatial attention actually mimics a spotlight (15) apply to our results as well. For example, our results tell us little about the shape or spatial extent

of spatially specific  $\alpha$ -band representations because the spatially specific activity we observed could reflect either a circular spotlight of attention around the target location or a vector of attention spanning from fixation to the target location. Similarly, it remains unclear whether it is possible to represent multiple remembered locations at once without representing locations in between them. We are optimistic that future studies using this technique will help answer these questions and facilitate a better understanding of the role of spatial attention in spatial working memory.

## ACKNOWLEDGMENTS

We thank Garvey Gregory and Sarika Shetty for assistance with data collection. We also thank Jason Rajsic, Sisi Wang, and Christopher Sundby for helpful discussions.

## GRANTS

The present work was supported by National Institutes of Health Grants R01-EY019882, R01-MH110378, P30-EY08126, and T32-EY007135 (to G.F.W.) and National Eye Institute Grant T32-EY007135 (to D.W.S.).

## DISCLOSURES

No conflicts of interest, financial or otherwise, are declared by the authors.

## AUTHOR CONTRIBUTIONS

D.W.S. and G.F.W. conceived and designed research; D.W.S. performed experiments; D.W.S. analyzed data; D.W.S., S.M.P., and G.F.W. interpreted results of experiments; D.W.S. prepared figures; D.W.S. drafted manuscript; D.W.S., S.P., and G.F.W. edited and revised manuscript; D.W.S., S.M.P., and G.F.W. approved final version of manuscript.

## ENDNOTE

At the request of the authors, readers are herein alerted to the fact that additional materials related to this manuscript may be found at <https://osf.io/t5n9z/>. These materials are not a part of this manuscript, and have not undergone peer review by the American Physiological Society (APS). APS and the journal editors take no responsibility for these materials, for the website address, or for any links to or from it.

## REFERENCES

- Hakim N, Adam KCS, Gunseli E, Awh E, Vogel EK. Dissecting the neural focus of attention reveals distinct processes for spatial

- attention and object-based storage in visual working memory. *Psychol Sci* 30: 526–540, 2019. doi:10.1177/0956797619830384.
2. Wang S, Rajsic J, Woodman GF. The contralateral delay activity tracks the sequential loading of objects into visual working memory, unlike lateralized alpha oscillations. *J Cogn Neurosci* 31: 1689–1698, 2019. doi:10.1162/jocn\_a\_01446.
  3. Awh E, Jonides J. Overlapping mechanisms of attention and spatial working memory. *Trends Cogn Sci* 5: 119–126, 2001. doi:10.1016/S1364-6613(00)01593-X.
  4. Awh E, Vogel EK, Oh S-H. Interactions between attention and working memory. *Neuroscience* 139: 201–208, 2006. doi:10.1016/j.neuroscience.2005.08.023.
  5. Chun MM, Turk-Browne NB. Interactions between attention and memory. *Curr Opin Neurobiol* 17: 177–184, 2007. doi:10.1016/j.conb.2007.03.005.
  6. Foster JJ, Bsales EM, Awh E. Covert spatial attention speeds target individuation. *J Neurosci* 40: 2717–2726, 2020. doi:10.1523/JNEUROSCI.2962-19.2020.
  7. Foster JJ, Sutterer DW, Serences JT, Vogel EK, Awh E. Alpha-band oscillations enable spatially and temporally resolved tracking of covert spatial attention. *Psychol Sci* 28: 929–941, 2017. doi:10.1177/0956797617699167.
  8. Rihs TA, Michel CM, Thut G. Mechanisms of selective inhibition in visual spatial attention are indexed by alpha-band EEG synchronization. *Eur J Neurosci* 25: 603–610, 2007. doi:10.1111/j.1460-9568.2007.05278.x.
  9. van Moorselaar D, Foster JJ, Sutterer DW, Theeuwes J, Olivers CNL, Awh E. Spatially selective alpha oscillations reveal moment-by-moment trade-offs between working memory and attention. *J Cogn Neurosci* 30: 256–266, 2017. doi:10.1162/jocn\_a\_01198.
  10. Ester EF, Nouri A, Rodriguez L. Retrospective cues mitigate information loss in human cortex during working memory storage. *J Neurosci* 38: 8538–8548, 2018. doi:10.1523/JNEUROSCI.1566-18.2018.
  11. Foster JJ, Sutterer DW, Serences JT, Vogel EK, Awh E. The topography of alpha-band activity tracks the content of spatial working memory. *J Neurophysiol* 115: 168–177, 2016. doi:10.1152/jn.00860.2015.
  12. Nouri A, Ester EF. Recovery of information from latent memory stores decreases over time. *Cogn Neurosci* 11: 101–110, 2019. doi:10.1080/17588928.2019.1617258.
  13. Sutterer DW, Foster JJ, Adam KCS, Vogel EK, Awh E. Item-specific delay activity demonstrates concurrent storage of multiple active neural representations in working memory. *PLoS Biol* 17: e3000239, 2019. doi:10.1371/journal.pbio.3000239.
  14. Sutterer DW, Foster JJ, Serences JT, Vogel EK, Awh E. Alpha-band oscillations track the retrieval of precise spatial representations from long-term memory. *J Neurophysiol* 122: 539–551, 2019. doi:10.1152/jn.00268.2019.
  15. Cave KR, Bichot NP. Visuospatial attention: beyond a spotlight model. *Psychon Bull Rev* 6: 204–223, 1999. doi:10.3758/bf03212327.
  16. Mangun GR, Hillyard SA. The spatial allocation of visual attention as indexed by event-related brain potentials. *Hum Factors* 29: 195–211, 1987. doi:10.1177/001872088702900207.
  17. Posner MI, Snyder CR, Davidson BJ. Attention and the detection of signals. *J Exp Psychol* 109: 160–174, 1980. doi:10.1037/0096-3445.109.2.160.
  18. Freeman J, Simoncelli EP. Metamers of the ventral stream. *Nat Neurosci* 14: 1195–1204, 2011. doi:10.1038/nn.2889.
  19. Desimone R, Albright TD, Gross CG, Bruce C. Stimulus-selective properties of inferior temporal neurons in the macaque. *J Neurosci* 4: 2051–2062, 1984. doi:10.1523/jneurosci.04-08-02051.1984.
  20. Schall JD, Morel A, King DJ, Bullier J. Topography of visual cortex connections with frontal eye field in macaque: convergence and segregation of processing streams. *J Neurosci* 15: 4464–4487, 1995. doi:10.1523/jneurosci.15-06-04464.1995.
  21. Sereno MI, Dale AM, Reppas JB, Kwong KK, Belliveau JW, Brady TJ, Rosen BR, Tootell RB. Borders of multiple visual areas in humans revealed by functional magnetic resonance imaging. *Science* 268: 889–893, 1995. doi:10.1126/science.7754376.
  22. Wandell BA, Brewer AA, Dougherty RF. Visual field map clusters in human cortex. *Philos Trans R Soc Lond B Biol Sci* 360: 693–707, 2005. doi:10.1098/rstb.2005.1628.
  23. Itthipuripat S, Sprague TC, Serences JT. Functional MRI and EEG index complementary attentional modulations. *J Neurosci* 39: 6162–6179, 2019. doi:10.1523/jneurosci.2519-18.2019.
  24. Popov T, Gips B, Kastner S, Jensen O. Spatial specificity of alpha oscillations in the human visual system. *Hum Brain Mapp* 40: 4432–4440, 2019. doi:10.1002/hbm.24712.
  25. Sprague TC, Ester EF, Serences JT. Restoring latent visual working memory representations in human cortex. *Neuron* 91: 694–707, 2016. doi:10.1016/j.neuron.2016.07.006.
  26. Sprague TC, Serences JT. Attention modulates spatial priority maps in the human occipital, parietal and frontal cortices. *Nat Neurosci* 16: 1879–1887, 2013. doi:10.1038/nn.3574.
  27. Feldmann-Wüstefeld T, Awh E. Alpha-band activity tracks the zoom lens of attention. *J Cogn Neurosci* 32: 272–282, 2020. doi:10.1162/jocn\_a\_01484.
  28. Bahramisharif A, Heskes T, Jensen O, van Gerven MAJ. Lateralized responses during covert attention are modulated by target eccentricity. *Neurosci Lett* 491: 35–39, 2011. doi:10.1016/j.neulet.2011.01.003.
  29. Roijndijk L, Farquhar J, van Gerven M, Jensen O, Gielen S. Exploring the impact of target eccentricity and task difficulty on covert visual spatial attention and its implications for brain computer interfacing. *PLoS One* 8: e80489, 2013. doi:10.1371/journal.pone.0080489.
  30. Foster JJ, Bsales EM, Jaffe RJ, Awh E. Alpha-band activity reveals spontaneous representations of spatial position in visual working memory. *Curr Biol* 27: 3216–3223.e6, 2017. doi:10.1016/j.cub.2017.09.031.
  31. Brainard DH. The psychophysics toolbox. *Spat Vis* 10: 433–436, 1997. doi:10.1163/156856897X00357.
  32. Pelli DG. The VideoToolbox software for visual psychophysics: transforming numbers into movies. *Spat Vis* 10: 437–442, 1997. doi:10.1163/156856897X00366.
  33. Lins OG, Picton TW, Berg P, Scherg M. Ocular artifacts in recording EEGs and event-related potentials II: source dipoles and source components. *Brain Topogr* 6: 65–78, 1993. doi:10.1007/BF01234128.
  34. Cohen MX. *Analyzing Neural Time Series Data: Theory and Practice*. Cambridge, MA: THE MIT Press, 2014. <https://doi.org/10.7551/mitpress/9609.001.0001>
  35. Sprague TC, Adam KCS, Foster JJ, Rahmati M, Sutterer DW, Vo VA. Inverted encoding models assay population-level stimulus representations. *eNeuro* 5: ENEURO.0098-18.2018, 2018. doi:10.1523/ENEURO.0098-18.2018.
  36. Sprague TC, Saproo S, Serences JT. Visual attention mitigates information loss in small- and large-scale neural codes. *Trends Cogn Sci* 19: 215–226, 2015. doi:10.1016/j.tics.2015.02.005.
  37. Suchow JW, Brady TF, Fougny D, Alvarez GA. Modeling visual working memory with the MemToolbox. *J Vis* 13: 9, 2013. doi:10.1167/13.10.9.
  38. Polyn SM, Norman KA, Kahana MJ. A context maintenance and retrieval model of organizational processes in free recall. *Psychol Rev* 116: 129–156, 2009. doi:10.1037/a0014420.
  39. Schwarz G. Estimating the dimension of a model. *Ann Statist* 6: 461–464, 1978. doi:10.1214/aos/1176344136.
  40. Maris E, Oostenveld R. Nonparametric statistical testing of EEG- and MEG-data. *J Neurosci Methods* 164: 177–190, 2007. doi:10.1016/j.jneumeth.2007.03.024.
  41. Corbetta M, Shulman GL. Control of goal-directed and stimulus-driven attention in the brain. *Nat Rev Neurosci* 3: 201–215, 2002. doi:10.1038/nrn755.
  42. Rosen ML, Stern CE, Michalka SW, Devaney KJ, Somers DC. Influences of long-term memory-guided attention and stimulus-guided attention on visuospatial representations within human intraparietal sulcus. *J Neurosci* 35: 11358–11363, 2015. doi:10.1523/JNEUROSCI.1055-15.2015.
  43. Haegens S, Cousijn H, Wallis G, Harrison PJ, Nobre AC. Inter- and intra-individual variability in alpha peak frequency. *Neuroimage* 92: 46–55, 2014. doi:10.1016/j.neuroimage.2014.01.049.
  44. Klimesch W, Schimke H, Pfurtscheller G. Alpha frequency, cognitive load and memory performance. *Brain Topogr* 5: 241–251, 1993. doi:10.1007/BF0128991.
  45. Mesulam MM. Spatial attention and neglect: parietal, frontal and cingulate contributions to the mental representation and

- attentional targeting of salient extrapersonal events. *Philos Trans R Soc Lond B Biol Sci* 354: 1325–1346, 1999. doi:[10.1098/rstb.1999.0482](https://doi.org/10.1098/rstb.1999.0482).
46. **Samaha J, Sprague TC, Postle BR.** Decoding and reconstructing the focus of spatial attention from the topography of alpha-band oscillations. *J Cogn Neurosci* 28: 1090–1097, 2016. doi:[10.1162/jocn\\_a\\_00955](https://doi.org/10.1162/jocn_a_00955).
47. **Kass RE, Raftery AE.** Bayes factors. *J Am Stat Assoc* 90: 773–795, 1995. doi:[10.2307/2291091](https://doi.org/10.2307/2291091).
48. **Cabeza R, Ciaramelli E, Olson IR, Moscovitch M.** The parietal cortex and episodic memory: an attentional account. *Nat Rev Neurosci* 9: 613–625, 2008. doi:[10.1038/nrn2459](https://doi.org/10.1038/nrn2459).
49. **Stokes MG, Atherton K, Patai EZ, Nobre AC.** Long-term memory prepares neural activity for perception. *Proc Natl Acad Sci USA* 109: E360–E367, 2012. doi:[10.1073/pnas.1108555108](https://doi.org/10.1073/pnas.1108555108).
50. **Sprague TC, Ester EF, Serences JT.** Reconstructions of information in visual spatial working memory degrade with memory load. *Curr Biol* 24: 2174–2180, 2014. doi:[10.1016/j.cub.2014.07.066](https://doi.org/10.1016/j.cub.2014.07.066).